COARSE-GRAINED POTENTIAL FOR INTERACTION WITH A SPHERICAL COLLOIDAL PARTICLE AND PLANAR WALL

Milan Předota[a,b,*], Ivo Nezbeda[b1,c] and Stanislav Pařez[b2]

[a] *Institute of Physics and Biophysics, Faculty of Science, University of South Bohemia, 370 05 České Budějovice, Czech Republic; e-mail: predota@prf.jcu.cz*

[b] *E. Hála Laboratory of Thermodynamics, Institute of Chemical Process Fundamentals, Academy of Sciences, v.v.i., 165 02 Prague 6, Czech Republic; e-mail: [1] ivonez@icpf.cas.cz, [2] parez@icpf.cas.cz*

[c] *Faculty of Science, J. E. Purkinje University, 400 96 Ústí nad Labem, Czech Republic*

Received November 3, 2009
Accepted February 8, 2010
Published online May 12, 2010

Dedicated to Professor Ivo Nezbeda on the occasion of his 65th birthday.

An effective coarse-grained interaction potential between a point particle and a spherical colloidal particle with continuously distributed inverse power-law interaction sites is derived. The potential covers all ranges of spherical particle size, from a point particle up to an infinitely large particle forming a planar surface. In the small size limit, the point-to-point interaction is recovered, while in the limit of an infinitely large sphere the potential comes over to the known particle–wall potentials as, e.g., the 9–3 potential in the case of the Lennard–Jones interaction. Correctness and usefulness of the derived potential is exemplified by its application to SPC/E water at a graphite sphere and wall.

Keywords: Spherical colloidal particles; Surface interaction; Effective coarse-grained potential; Molecular simulations; Water at graphite surface.

The knowledge of the structure (both spatial and orientational) of fluids at solid and liquid surfaces is of great importance from both the technological and scientific points of view. There are two most common cases of such inhomogeneous fluids: (i) fluids in confinement[1] and (ii) bulk fluid in equilibrium with the surface[2] or even in non-equilibrium, e.g., the condensation of vapor on droplets of aerosols particles. An example of the former case is fluid in pores or slits, and of the latter an (infinitely) diluted solution with the solute, e.g., a colloidal particle, playing the role of a solid object. Of a particular interest in this case is the structure of water around large biomolecules, i.e., non-planar surface[3].

doi:10.1135/cccc2009542

The structure of the fluid is affected by two main factors: the intermolecular interactions and the geometry of the surface. The interaction of a fluid molecule with the surface is given, in general, by its interaction with all atoms/molecules of the surface, including atoms/molecules at the interface as well as those underneath. Thus, regardless whether the surface is formed by nanoparticles, cavities, nanotubes or a macroscopic object, when it is modeled explicitly the resulting interaction potential of the surface with another component of the system (e.g., ion or molecule) is given by the sum of the direct atom–atom pair contributions. However, in some cases as, e.g., when the solid atoms are relatively small and closely packed, or when it is the presence of the surface itself which is more important then the specific individual atom–atom interactions, the surface can be treated as structureless and the sum can be replaced by an effective interaction which is, typically, a function of only two spatial variables (aside of the atom–atom interaction parameters), namely the distance from the surface and the curvature of the surface given by the particle radius (see, e.g., refs[4,5] and references therein). Of particular interest to us will be the limiting case of infinitely large spherical particle, which comes over to planar surface (half-space), both mathematically and physically as demonstrated by the observation of the change in the structure of the interfacial fluid adjacent to the particle.

For surfaces and interactions, which are modeled by potentials with a hard core, for instance, such as hard spheres and hard wall, the transition from a spherical to a planar interface is straightforward, because the condition preventing the point particle to overlap with the spherical particle is replaced by the corresponding condition excluding the penetration into the planar wall. We used this approach successfully studying the behavior of primitive water next to solutes modeled as hard spheres of different diameters including the limiting case of a planar hard wall[6,7] and demonstrated the continuous transition of density profiles of water next to the solute throughout these solutes sizes.

On a more realistic level, the non-electrostatic site–site interactions are commonly described by a combination of power law potentials, with the Lennard–Jones (LJ) potential being a general standard for describing both short-range core repulsions and attractions at medium separations. However, unlike the previous case of hard-core particles, considering one LJ particle as a point solute and increasing its length-scale parameter σ does not lead to the well-known case of the LJ fluid at the LJ 9–3 wall: (i) for finite values of σ, the interaction potential of the fluid molecule with such a spherical particle diverges to infinity only when the location of the particle

and solvent atom coincides, i.e., the particle is still point-wise; (ii) increasing σ leads to larger excluded volume of the particle, but concurrently to smearing of the potential, i.e., the slope of the potential decreases and the surface or the effective diameter of the particle (if something like that can be defined for point particles) becomes ill-defined. An example demonstrating this behavior is Fig. 1 of our paper[8], which shows smearing of the LJ solute–solvent pair correlation function when the solute diameter is increased up to ten times that of water. Carrying out the limit $\sigma \to \infty$ would lead to a particle which would repel all other components of the system to infinity, but at the same time the transition of the attractive to repulsive potential would be infinitely 'soft' and long-ranged. Consequently, such a limiting case is far from the flat solid surface, which features steep repulsion when approached by the solvent molecule.

The above problem lead us in ref.[8] to include the standard 9–3 interaction potential of a LJ wall in comparison with large LJ solutes. However, the results presented there make it clear that such a comparison is not adequate, and the graphs manifested that the behavior at the 9–3 wall is not the correct limiting case of a large LJ solute. The problem addressed in this paper is thus to find a potential between a point particle and a spherical colloidal particle such that in the case of the limit of an infinite sphere diameter we get the known effective interaction between a point particle and a flat wall.

The coarse-grained potentials between interacting bodies have been studied for a number of geometries, though often restricting to r^{-6} dispersion term only. Long time ago, the potential between two spherical particles interacting with r^{-6} potential was derived by Hamaker[9], including the limiting case of sphere interacting with a sphere of infinite diameter, i.e., planar half-space. Sixty years later, the potential between two spherical particles interacting with r^{-12} potential was derived by Henderson and co-workers[10], resulting in cumbersome analytical solution, which was further simplified by Dobruskin[11]. These two results combined lead to an interaction potential between colloidal particles based on LJ atom–atom interaction. The extension of Hamaker's solution[6] for r^{-6} potential to composite spheres consisting of inner and outer layers of different material is available[12]. The interaction potential between a point particle and an infinitely long cylinder (fiber), motivated by study of interaction of aerosol particles with fibrous filters was given[13] for general power-law potential r^{-m} leading to expression involving beta-function and hypergeometric function. Conveniently, simple algebraic formulas for both London potential r^{-6} and the asymptotic r^{-7} fully retarded vdW potential were given as well[13]. The inte-

grated r^{-6} interaction between a spherical particle and an infinite cylinder was later extended to the r^{-m} interaction[14], ending up for even m in an analytical solution containing complete elliptic integrals. Of closest interest for us, as part of the derivation[14], the interaction energy of a point particle with a sphere and a cylinder for interaction potential r^{-m} was given in terms of hypergeometric function. The resulting simple formulas for a sphere and $m = 6$ or 7, as well as for a cylinder and $m = 7$ were also given[14]. As an example of more complex geometries, the r^{-6} interaction between two torus-shaped colloidal particles was also investigated[15].

THEORY

The interaction between two point particles is commonly described by a combination of the power law potentials, with the LJ potential,

$$u_{\mathrm{LJ}}(r) = 4\varepsilon\left[\left(\frac{\sigma}{r}\right)^{12} - \left(\frac{\sigma}{r}\right)^{6}\right] \qquad (1)$$

being the standard one for describing both the core repulsions and attractions at medium separations. It is tempting to mimic the transition from the spherical particle to a planar wall by performing the limit $\sigma \to \infty$ but, as explained above, this procedure does not lead to the case of a particle of increasing diameter D ($D = 2R$) and atomistically filled (in our simplification, continuously on the mesoscopic scale) with atoms of constant material-related interaction parameters ε and σ independent of the particle size. On the contrary, we will proceed by keeping the parameters ε and σ constant and perform the summation of the interaction potential of a point particle with the spherical particle implicitly by integrating the interaction potential over its volume given by diameter D, resulting in a still rather simple mathematical expression for an effective pair potential between the spherical and point particles. As will be demonstrated, such a potential will lead, for sufficiently steep repulsion, to divergence of the mutual interaction when the point particle approaches the surface of the spherical particle, and to the 9–3 interaction with a flat LJ wall in the limit $D \to \infty$.

We need to calculate the interaction of a spherical particle of radius R filled continuously with the matter of number density ρ interacting with a point atom at distance r from its center. The derivation is given for the interaction potential between the continuous matter and the point atom in the form $u(x) = x^{-n}$, $n \neq 2, 3, 4$, which covers the most interesting cases of the Coulombic and LJ interactions. The derivation, detailed in Appendix, is

carried out in two steps: (i) the effective potential between a point particle and an infinitely thin spherical shell is derived first, and then (ii) the potential of the entire sphere is obtained by integration over the shells up to the desired diameter. The resulting interaction between the sphere and the point particle assumes thus the form

$$U(r,D) = \frac{2\pi\rho}{2-n}\left[\frac{(r+D/2)^{4-n} - (r-D/2)^{4-n}}{(4-n)r} - \frac{(r+D/2)^{3-n} - (r-D/2)^{3-n}}{3-n}\right] \quad (2)$$

where r is the distance between the center of the colloidal sphere and the point particle. The number density of interacting sites within the sphere, ρ, can be easily calculated from the mass density and molar mass of the material constituting the sphere.

The above potential can be expressed alternatively as a function of distance $z = r - D/2$ between the surface of the sphere and the point atom (e.g., atom of the water molecule solvating the sphere)

$$U(z,D) = \frac{2\pi\rho}{2-n}\left[\frac{(z+D)^{4-n} - z^{4-n}}{(4-n)(z+D/2)} - \frac{(z+D)^{3-n} - z^{3-n}}{3-n}\right]. \quad (3)$$

For the particular case of the matter interacting via the LJ potential (*1*), the above formulas become

$$U_{\mathrm{LJ}}(r,D) = 4\pi\varepsilon\rho\sigma^6\left\{\frac{\sigma^6}{5}\left[\frac{(r+D/2)^{-8} - (r-D/2)^{-8}}{8r} - \frac{(r+D/2)^{-9} - (r-D/2)^{-9}}{9}\right] - \right.$$

$$\left. - \frac{1}{2}\left[\frac{(r+D/2)^{-2} - (r-D/2)^{-2}}{2r} - \frac{(r+D/2)^{-3} - (r-D/2)^{-3}}{3}\right]\right\} \quad (4)$$

and

$$U_{\mathrm{LJ}}(z,D) = 4\pi\varepsilon\rho\sigma^6\left\{\frac{\sigma^6}{5}\left[\frac{(z+D)^{-8} - z^{-8}}{8(z+D/2)} - \frac{(z+D)^{-9} - z^{-9}}{9}\right] - \right.$$

$$\left. - \frac{1}{2}\left[\frac{(z+D)^{-2} - z^{-2}}{2(z+D/2)} - \frac{(z+D)^{-3} - z^{-3}}{3}\right]\right\}. \quad (5)$$

This expression can be expressed alternatively as

$$U_{\mathrm{LJ}}(z,D) = 4\pi\varepsilon\rho\sigma^6 D^3 \times$$

$$\times\left[\frac{\sigma^6}{180}\frac{4D^6 + 27zD^5 + 81z^2D^4 + 138z^3D^3 + 144z^4D^2 + 90z^5D + 30z^6}{z^9(z+D)^9} - \right.$$

$$\left. - \frac{1}{6z^3(z+D)^3}\right]. \qquad (6)$$

While the first cumbersome term originating from the x^{-12} potential is an alternative representation of the corresponding term given by Dobruskin[11], the second term originating from the x^{-6} potential simplifies nicely (after trivial substitution of variables) to the form derived the same year by Dobruskin[11] and Kirsch[14].

Let us discuss now several interesting limiting cases of Eqs (*2*) and (*3*).

1. Infinitely large sphere $D \to \infty$, which becomes a semi-infinite wall.

In this case, it is convenient to express the potential as the function of the distance z from the surface, Eq. (*3*). For $D \to \infty$, only the last term is non-zero for $n > 4$, i.e.,

$$U(z,\infty) = \lim_{D\to\infty} U(z,D) = \frac{2\pi\rho}{2-n}\left[\frac{z^{3-n}}{3-n}\right]. \qquad (7)$$

For the LJ potential, the resulting potential

$$U_{\mathrm{LJ}}(z,\infty) = \lim_{D\to\infty} U_{\mathrm{LJ}}(z,D) =$$

$$= 8\pi\varepsilon\rho\sigma^3\left[\frac{(\sigma/z)^9}{9.10} - \frac{(\sigma/z)^3}{3.4}\right] = 4\pi\varepsilon\rho\sigma^3\left[\frac{(\sigma/z)^9}{45} - \frac{(\sigma/z)^3}{6}\right] \qquad (8)$$

becomes the well-known LJ 9–3 point–wall interaction potential. The dependence of the interaction with a spherical LJ particle of diameter D as a function of the distance from the surface is plotted in Fig. 1. The potential diverges at contact distance $z = 0$. For large diameters, the curves approach

the interaction with a flat LJ wall (Eq. (*8*)). For small particles, the magnitude of the interaction decreases as D^3 due to the limited mass of the sphere.

2. Limiting case of a small sphere.

In this case, a more appropriate option is to express the potential as a function of the distance r from the center of sphere (Eq. (*2*)); particularly in a situation when the comparison with the point LJ particle is of interest. In this way, one can easily answer the question what is the effect of the finite diameter of the sphere as opposed to a point LJ particle. The limit $D << r$ leads, within the first non-zero term in D, to the expression $U(r,d << r) = \pi\rho D^3/6r^n = V\rho/r^n$, i.e., the interaction with the sphere reduces to the interaction with a point particle located in the center of the sphere and proportional to the total mass (number density times volume) of the sphere. In Fig. 2, the interaction potentials with a finite-size sphere of diameter D (full symbols) are compared with the point particle of the same 'mass' (open symbols), i.e., the product $V\rho$ is the same in both cases and the potential for the point LJ particle is calculated as

$$U_{\mathrm{LJ}}^{\mathrm{point}}(r,D) = \frac{\pi\rho D^3}{6} U_{\mathrm{LJ}}(r) = V\rho U_{\mathrm{LJ}}(r) \,. \qquad (9)$$

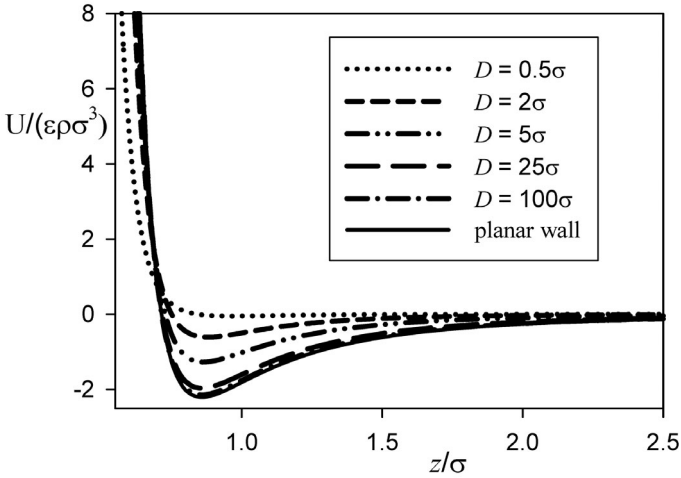

FIG. 1
Dependence of the interaction with a spherical LJ particle of diameter D and a planar LJ wall as a function of the distance from the surface z

At distances $r >> D$, both potentials become indistinguishable, i.e., the finite size of the sphere is not important and the interaction potential can be approximated by the point LJ potential. At distances comparable to the diameter of the sphere, the behavior of both types of curves is significantly different. The potential $U_{LJ}(r,D)$ given by Eq. (*4*) diverges to infinity at the contact distance $D/2$, while the point LJ potential (*9*) diverges at 0. As a result, the potential of a finite sphere is steeper in the repulsive region. At the same time, at larger distances, the potential of the sphere is more attractive compared to the LJ potential, due to the interaction with the closest part of the sphere, i.e., the interaction with its atoms, which are closer than the center, i.e., assumed location of the point LJ particle. This behavior is caused by the short-range nature of the LJ interaction.

3. As an exercise, one can verify that for $n = 0$, Eq. (*2*) yields a trivial result

$$U(r,D) = \frac{\pi\rho D^3}{6} = V\rho \qquad (10)$$

and for $n = 1$, it yields $U(r,D) = \pi\rho D^3/6r = V\rho/r$, i.e., the interaction with the sphere (outside of the sphere) depends only on its total mass and not on the radius, which is well-known for electrostatic and gravitational radial fields.

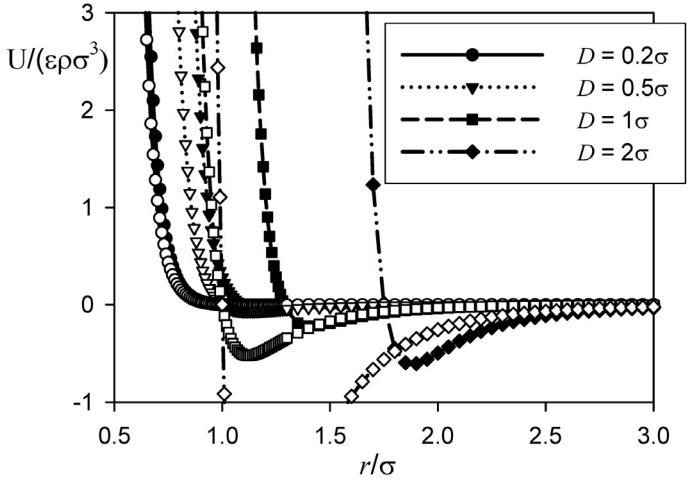

FIG. 2
Comparison of the interaction potential of finite sphere (Eq. (*4*), full symbols) with interaction potential of point LJ particle of the same 'mass' (Eq. (*9*), open symbols)

SIMULATION RESULTS

As a representative system to demonstrate the dependence of structural properties on the size of the spherical solute, we have chosen SPC/E water[16] in contact with a carbon (graphite) sphere of mass density 2.25 g cm^{-3}, which corresponds to number density $\rho = 112.9125$ nm^{-3}. The interaction parameters of carbon, $\sigma_C = 0.34$ nm and $\varepsilon_C/k_B = 28$ K, were taken from ref.[4]. The Lorentz–Berthelot combining rules were applied for the carbon–oxygen parameters, which are used in the calculation of the van der Waals interactions between the sphere and water. The resulting potential, as well as its first derivative, were tabulated and used as input for simulations in GROMACS[17]. Particle-mesh Ewald summation was used to treat the long-range electrostatic interactions, Berendsen thermostat and barostat were applied to keep average temperature 300 K and pressure 1 bar, respectively. The interaction cutoff was larger then $D/2 + 1.2$ nm to allow interaction between the sphere and water molecules up to distance 1.2 nm from the sphere surface. Since setting independent cutoffs for sphere–water and water–water interactions was not achieved in GROMACS, the same cutoff was applied in both cases, though leading to unneccessary increase of CPU time. In all cases, there was only one spherical solute in the simulation box, solvated by water molecules. The overview of the simulation parameters is given in Table I. The simulation time can be lower for larger spheres, as

TABLE I
Parameters of simulations

D, σ	D, nm	r_{cut}, nm	L, nm	N	m_{sphere}, m_u	t_{sim}, ns	t_{conf}, ps
0.5	0.1583	1.30	3.00	894	18	100	1
1	0.3166	1.40	3.49	1410	18	73	1
2	0.6332	1.55	3.50	1410	144	56	1
5	1.583	2.05	4.55	3009	2250	12.5	0.5
10	3.166	2.80	5.83	5832	18000	6	0.5
planar wall	–	0.9	3.166 (xy) 2.963 (z)	864	–	1	–

Diameter of the sphere D given as multiple of the LJ σ parameter of the SPC/E potential and in absolute terms, interaction cutoff radius r_{cut}, average box length L, number of water molecules N, mass of sphere m_{sphere}, simulation time t_{sim}, and interval between saving of configurations for post-processing t_{conf}

their larger surface implies more molecules in their vicinity and therefore better statistics compared to small spheres. The mass of the sphere, a parameter without a direct effect on the results, is proportional to the volume of the sphere; only in the case of the smallest sphere the mass was kept at the value 18 m_u to prevent potentially too vivid motion of the sphere. Radial distribution functions and angular distributions of water molecules were obtained by the analysis of saved configurations at t_{conf} intervals. Our previous Monte Carlo results[8] for the case of planar 9–3 wall were used. The latter results were obtained by our own code with every configuration analyzed during the simulation run.

The radial distribution functions between the center of the sphere and the oxygen atom of the water molecule for differently sized spheres (Fig. 3, top) shows the obvious effect of the sphere size. However, unlike our previous work[8], in which the size of the sphere was modeled by enlarging the LJ σ parameter, in the current case the interface between the sphere and solvent is well defined (as space occupied/unoccupied by the continuously distributed atoms forming the sphere) and the shape of the curves is very similar for all solute sizes. This is even better demonstrated by the bottom plot of Fig. 3, where the curves are plotted as a function of distance from the surface of the sphere; in this case the density profile at the planar wall is included as well. The continuous trend of the curves with the enlarging solute diameter towards the density profile at the planar wall is evident. Smaller sphere allows closer approach of water towards its surface as, due to larger curvature of the surface, fewer atoms participates in the repulsion compared to the planar wall. Figure 3 also indicates the split of the first solvation shell into two subshells **Ia** and **Ib**, for which the angular distribution of water molecules was analyzed in detail. Due to the similarity of all curves, common dividing points 0.286 nm (first peak) and 0.482 nm (first minimum after the first peak) were used for all solute sizes, though a slight continuous shift of the minimum towards larger distances with the increasing solute size is present. Interesting phenomenon is the height of the first peak which is not monotonous, but exhibits maximum in the 2–5σ solute range, which must be linked with the most convenient packing and/or hydrogen bonding structure of water molecules at these surfaces.

The angular distribution of water molecules in the vicinity of the solute can be unambiguously described by angular bivariate plots[8,18], which uniquely describe the orientation of the water molecule relative to the normal of the surface (center of sphere–oxygen vector) in terms of cos θ, where θ is the vector between the surface normal and dipole vector of the molecule, and angle ϕ, formed by the projection of the surface normal to the

plane perpendicular to the molecule dipole moment. For details and schematic figures, see the original paper[18]. The bivariate plots for differently sized spheres and the planar wall (Fig. 4) shows first of all that orientation changes are evident in the **Ia** subshell, while the structure of subshell **Ib** does not change significantly. With the help of numbering selected orientations of water molecules relative to the solute (Fig. 5) and their location on

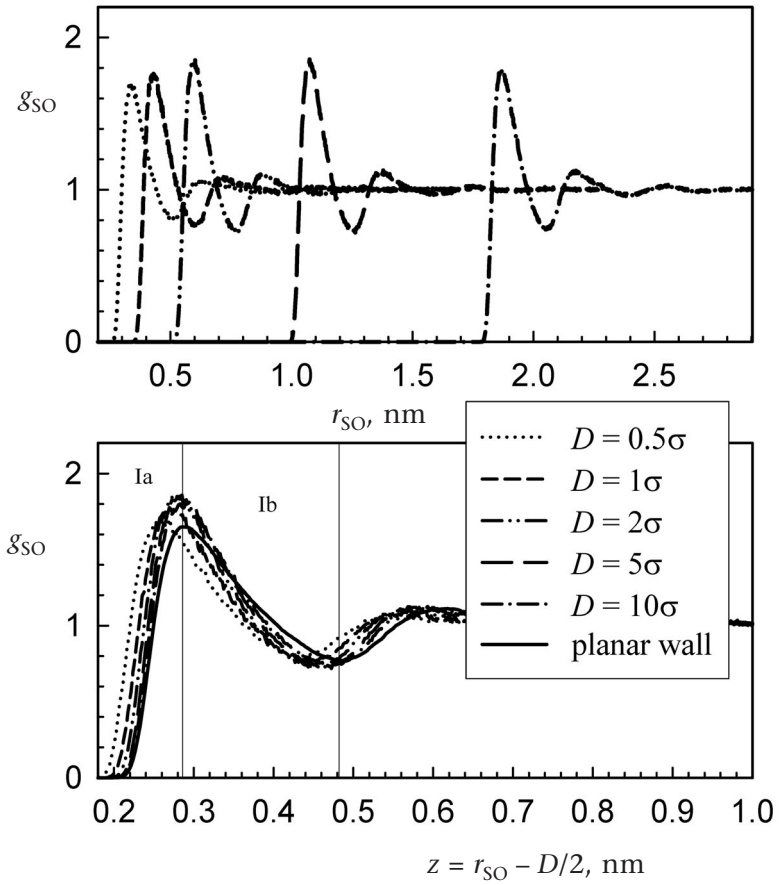

FIG. 3
Sphere–oxygen radial distribution functions for differently sized spheres as a function of distance from the center (top) and surface (bottom) of the sphere. The density profile at planar wall is included in the latter case

bivariate plots (Fig. 4), the effect of the increasing solute size can be identified as decreasing population of the orientation **I** with two hydrogens and one lone-pair site straddling the sphere, and orientation **II** with one hydrogen site and two lone-pair sites straddling the sphere. At the same time, orientation **III** with the molecular plane of water parallel to the surface becomes predominantly populated. The transition from the largest sphere studied, $D = 10\sigma$, towards the planar wall leads to even further reorientation of water molecules, with configurations **V** and **VI**, both pointing with the hydrogen site or the lone-pair site toward the surface and sacrificing the hydrogen bond of this site, clearly distinguishable, though secondary to population of configuration **III**. Overall we see a significant reorientation in the **Ia** subshell, while only small changes are seen in the **Ib** subshell.

In Fig. 6, we present the monovariate distribution of cos θ, defined identically as in the case of bivariate plot, i.e., the monovariate plot represents

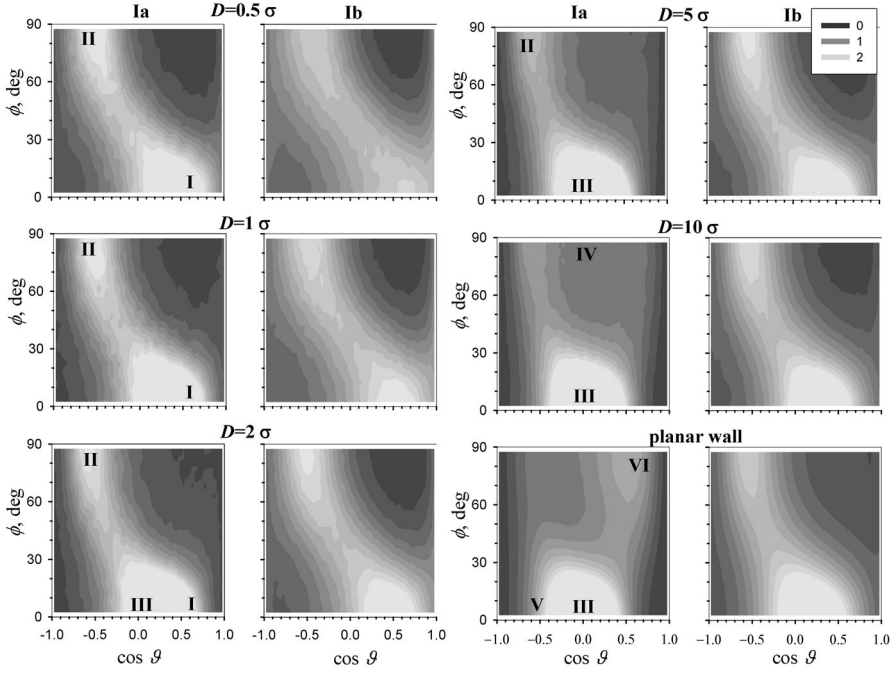

FIG. 4
Bivariate plots of angular distribution of water molecules around differently sized spheres and planar wall

projection of the bivariate plot when the vertical ϕ axis is collapsed. While the increase, with the increasing solute size, of the population of orientations with the dipole moment parallel to the surface is captured by the monovariate plot, other phenomena, particularly shift from orientations **I** to **VI** and **II** towards **V** or difference between orientations **III** and **IV** can not be addresses by this type of plot, as these pairs of different orientations result in identical dipole orientations. We have addressed this deficiency of the monovariate plots, particularly of the dipole orientation, earlier[8], but it is probably worth stressing this again. The monovariate distribution of angle α, defined as angle between the oxygen–sphere vector and OH vector of the molecule, is much more informative in terms of indicating the trends discussed on bivariate plots. Particularly, the shift of the populations of orientations **I** and **II** towards **III**, or even **V** and **VI**, when the solute is enlarged, is well captured.

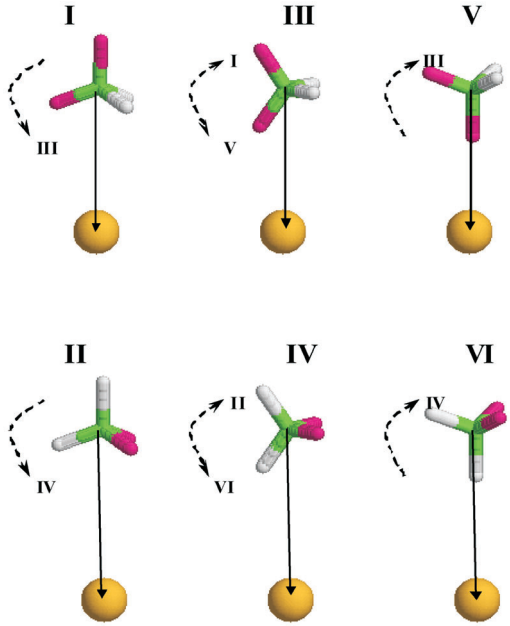

FIG. 5
Illustration of the identified orientations **I–VI** of the water molecules relative to the solute. The white and dark grey sticks indicate the O–H bonds and the lone pair directions, respectively. The reference vector pointing from the water oxygen to the solute is also shown. The curved arrows show the rotation that transforms the given orientation to the indicated one

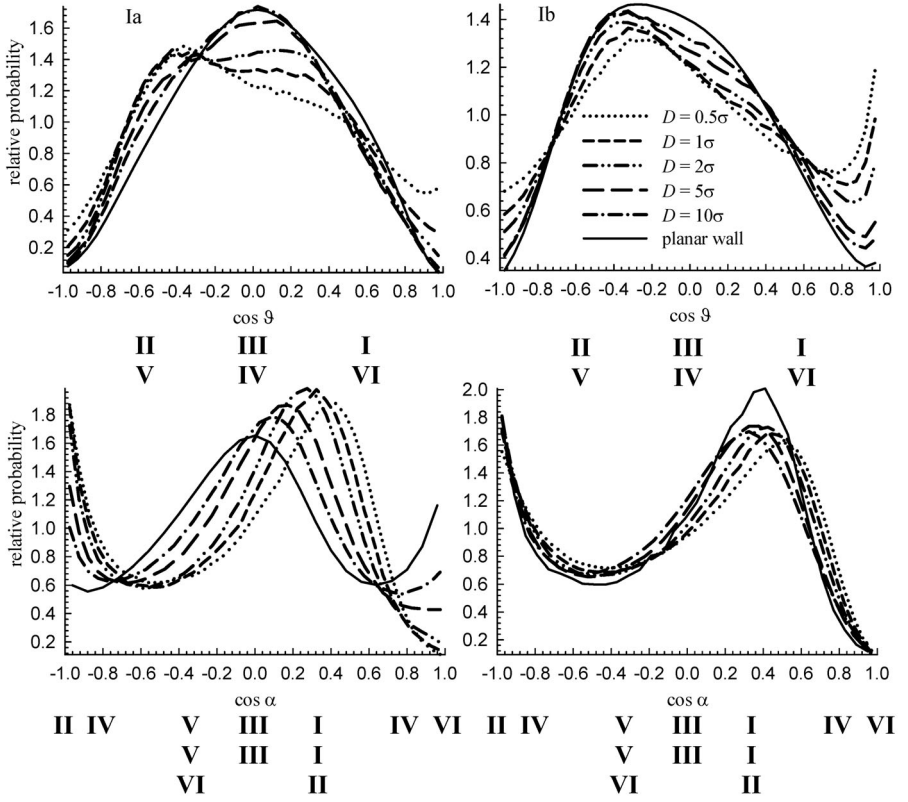

FIG. 6
Monovariate plots of angular distribution of water molecules around differently sized spheres and planar wall

CONCLUSIONS

We have derived, in a simple analytical form, the coarse-grained potential for the interaction between a finite size spherical colloidal particle, formed by homogeneously distributed sites interacting with r^{-n} potential, and a point particle. We have demonstrated the correct limiting behavior for large spheres, which approaches the behavior of a planar surface. For sufficiently steep potentials, with repulsion steeper than r^{-4}, the resulting interaction preserves the rigidity of the particle, i.e., the interaction diverges when the point particle approaches the surface of the spherical particle.

The resulting integrated potential might be used successfully in situations when the diameter of the sphere becomes large compared to the interatomic distances of atoms forming the sphere and in the absence of specific interactions with the surface (such as, e.g., special surface groups, charged atoms, etc.), i.e., in situation when the steric van der Waals interaction is dominant. The advantages of the derived potential are twofold: (i) when appropriate, it allows avoiding the all-atom modeling of the sphere by replacing the interaction with a coarse-grained potential and making thus simulations more efficient; (ii) it enables a systematic study of the effect of the particle size and its curvature on the properties of the interface at its surface. Representative results demonstrating suitability of the approach were presented for the model case of carbon sphere and planar surface in contact with SPC/E water.

We demonstrate a transition between the potentials for colloidal bodies of various geometries discussed in the introduction and the extensively explored 9–3 LJ potential for effective interaction with semi-infinite planar wall and further modifications of Steele's potential[4,19]. Our results capture the smooth change of the interfacial structure of water in contact with spherical particle of increasing size including the limiting case of planar surface, as documented by the density distribution functions and the orientation distributions, described unambiguously by the bivariate plots, which are superior to the less instructive monovariate plots.

There is another class of coarse-grained potentials closely related to the one investigated here, namely the coarse-grained interaction potential of a point atom with fullerene C_{60}–C_{96} buckyballs[20,21], i.e., cage-like structures with all carbon atoms on the surface of a sphere. The coarse-grained potential in this case arises from assumption of homogeneous distribution of carbon atoms on the surface of the buckyball, which is well justified due to the large number of these atoms. In fact the first step of the derivation of our coarse-grained interaction potential between a point and filled sphere, which is interaction between a point and a spherical surface, is a generic case of Eq. (*1*) of ref.[20], with the latter being a special case of LJ interaction. The coarse-grained interaction between two carbon buckyballs, known as Girifalco potential[22], has been derived even earlier by integrating interaction between two spherical surfaces. The coarse-grained interaction potential with cylindrical wall was derived recently[23].

As a tribute to the seminal work of Hamaker[9], we conclude this paper by reporting his result for the interaction potential between two spherical colloidal particles of diameters $D_1 = 2R_1$ and $D_2 = 2R_2$ and center-to-center sep-

aration r, i.e., surface-to-surface distance $z = r - R_1 - R_2$, with atom–atom interaction $-A/x^6$,

$$U(r,R_1,R_2) = \frac{-A\pi^2\rho^2}{6} \times$$

$$\times \left[\frac{2R_1R_2}{r^2 - (R_1 + R_2)^2} + \frac{2R_1R_2}{r^2 - (R_1 - R_2)^2} + \ln \frac{r^2 - (R_1 + R_2)^2}{r^2 - (R_1 - R_2)^2} \right] \qquad (11)$$

or alternatively,

$$U(z,D_1,D_2) = \frac{-A\pi^2\rho^2}{6} \times$$

$$\times \left[\frac{D_1D_2 \,/\, 2}{z^2 + z(D_1 + D_2)} + \frac{D_1D_2 \,/\, 2}{z^2 + z(D_1 + D_2) + D_1D_2} + \ln \frac{z^2 + z(D_1 + D_2)}{z^2 + z(D_1 + D_2) + D_1D_2} \right]. \qquad (12)$$

This research was supported by the Czech Science Foundation Research (project No. 203/08/0094), by the Grant Agency of the Academy of Sciences of the Czech Republic (project No. IAA400720802), and by the Ministry of Education, Youth and Sports of the Czech Republic (project No. ME09062).

REFERENCES

1. Gelb L. D., Gubbins K. E., Radhakrishnan R., Sliwinska-Bartkowiak M.: *Rep. Prog. Phys.* **1999**, *62*, 1573.
2. Henderson D. (Ed.): *Fundamentals of Inhomogeneous Fluids*. Dekker, New York 1992.
3. Oleinikova A., Brovchenko I.: *Mol. Phys.* **2006**, *104*, 3841.
4. Steele W. A.: *The Interaction of Gases with Solid Surfaces*. Pergamon Press, Oxford 1974.
5. Jakubov T. S., Mainwaring D. E.: *Physica B: Condens. Matter* **2006**, *381*, 57.
6. Předota M., Nezbeda I.: *Mol. Phys.* **1999**, *96*, 1237.
7. Předota M., Nezbeda I., Cummings P. T.: *Mol. Phys.* **2002**, *100*, 2189.
8. Jedlovszky P., Předota M., Nezbeda I.: *Mol. Phys.* **2006**, *104*, 2465.
9. Hamaker H. C.: *Physica* **1937**, *4*, 1058.
10. Henderson D., Duh D.-M., Chu X., Wasan D.: *J. Colloid Interface Sci.* **1997**, *185*, 265.
11. a) Dobruskin V. Kh.: *Langmuir* **2003**, *19*, 4004; b) Dobruskin V. Kh.: *Langmuir* **2005**, *21*, 2887.
12. Chan D. Y. C., Henderson D.: *IBM J. Res. Dev.* **1985**, *29*, 11.
13. Kirsh V. A.: *Colloid J.* **2000**, *62*, 714.
14. Kirsch V. A.: *Adv. Colloid Interface Sci.* **2003**, *104*, 311.

15. Ohshima H., Hyono A.: *J. Colloid Interface Sci.* **2009**, *332*, 251.
16. Berendsen H. J. C., Grigera J. R., Straatsma T. P.: *J. Phys. Chem.* **1987**, *91*, 6269.
17. Van Der Spoel D., Lindahl E., Hess B., Groenhof G., Mark A. E., Berendsen H. J. C.: *J. Comput. Chem.* **2005**, *26*, 1701.
18. Jedlovszky P., Vincze Á., Horvai G.: *J. Chem. Phys.* **2002**, *117*, 2271.
19. Steele W. A.: *Surf. Sci.* **1973**, *36*, 317.
20. Choudhury N.: *J. Chem. Phys.* **2006**, *125*, 034502.
21. Abramo M. C., Caccamo C., Costa D., Pellicane G., Ruberto R.: *Phys. Rev. E* **2004**, *69*, 031112.
22. Girifalco L. A.: *J. Phys. Chem.* **1992**, *96*, 858.
23. Zhang X., Wang W., Jiang G.: *Fluid Phase Equilib.* **2004**, *218*, 239.

APPENDIX

Derivation of the interaction potential between a point particle and spherical particle with a center at distance r and radius R continuously filled with a matter with number density ρ, interacting with potential $u(x) = x^{-n}$.

The derivation proceeds in two steps: 1. interaction $U_S(r,R')$ with a surface of a sphere with radius R' is derived, then 2. integration of the previous result for R' between 0 and R yields the resulting interaction $U(r,R)$ with a filled sphere, $U(r,R) = \int_0^R U_S(r,R')\,\mathrm{d}R'$.

1. Interaction with the spherical surface of surface number density of interaction sites $\kappa = \rho\,\mathrm{d}R'$ is integrated over spherical rings as shown in Fig. 7, i.e.,

$$U_S(r,R') = \frac{\mathrm{d}U(r,R)}{\mathrm{d}R'} = \int_{s=-R'}^{R'} u(x(s))\rho\,\mathrm{d}S = 2\pi R'\rho\int_{s=-R'}^{R'} u(x(s))\,\mathrm{d}s\,.$$

The relation between the interaction distance x and s is as follows

$$x^2 = (r-s)^2 + R'^2 - s^2 = r^2 - 2rs + R'^2 \Rightarrow 2x\,\mathrm{d}x = -2r\,\mathrm{d}s\,.$$

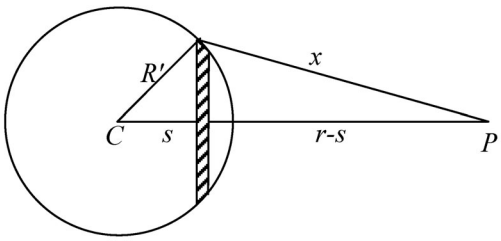

FIG. 7
Schematics of the variables defined to derive the interaction between point-wise particle located at P and a surface of a sphere of radius R' centered at C at a distance r

This allows carrying out the integration over x,

$$U_S(r,R') = 2\pi R'\rho\int_{s=-R'}^{R'} u(x(s))\,\mathrm{d}s = 2\pi R'\rho\int_{x=r+R'}^{r-R'} \frac{xu(x)}{-r}\,\mathrm{d}x =$$

$$= \frac{2\pi R'\rho}{r}\int_{x=r-R'}^{r+R'} xu(x)\,\mathrm{d}x = \frac{2\pi R'\rho}{r}\int_{x=r-R'}^{r+R'} x^{1-n}\,\mathrm{d}x =$$

$$= \frac{2\pi R'\rho}{r}\,\frac{(r+R')^{2-n} - (r-R')^{2-n}}{2-n} = U_S(r,R',+1) - U_S(r,R',-1)$$

where

$$U_S(r,R',\alpha) = \frac{2\pi R'\rho}{r}\,\frac{(r+\alpha R')^{2-n}}{2-n}\,.$$

Note that application of this generic formula for LJ potential leads to the frequently used interaction potential between a point and a homogeneously distributed LJ atoms along a surface of a sphere, Eq. (*1*) of ref.[20], used for the coarse-grained description of carbon buckyballs.

2. Similarly as the surface interaction was split into two contributions differing only by the sign, the interaction with the sphere will be split into corresponding two terms

$$U(r,R) = \int_0^R U_S(r,R')\,\mathrm{d}R' = U(r,R',+1) - U(r,R',-1)$$

where

$$U(r,R,\alpha) = \int_0^R I_S(r,R',\alpha)\,\mathrm{d}R' = \frac{2\pi\rho}{r(2-n)}\int_0^R R'(r+\alpha R')^{2-n}\,\mathrm{d}R'.$$

Carrying out substitution $r + \alpha R' = y$ (and considering $\alpha^2 = 1$) yields

$$U(r,R,\alpha) = \frac{2\pi\rho}{r(2-n)}\int_r^{r+\alpha R} (y-r)y^{2-n}\,\mathrm{d}y =$$

$$= \frac{2\pi\rho}{r(2-n)}\left[\frac{(r+\alpha R)^{4-n} - r^{4-n}}{4-n} - r\,\frac{(r+\alpha R)^{3-n} - r^{3-n}}{3-n}\right] =$$

$$= \frac{2\pi\rho}{2-n}\left[\frac{(r+\alpha R)^{4-n} - r^{4-n}}{r(4-n)} - \frac{(r+\alpha R)^{3-n} - r^{3-n}}{3-n}\right].$$

Finally, in the difference $U(r,R) = U(r,R,+1) - U(r,R,-1)$, the terms independent of α cancel out, leading to

$$U(r,R) = \frac{2\pi\rho}{2-n}\left[\frac{(r+R)^{4-n} - (r-R)^{4-n}}{r(4-n)} - \frac{(r+R)^{3-n} - (r-R)r^{3-n}}{3-n}\right].$$